

The Effect of Subgrade Cavity on Pavement. A Case Study

Mauro Coni(✉), Silvia Portas, James Rombi, and Francesca Maltinti

DICAAR, Department of Civil Engineering, Environment and Architecture, Faculty of Engineering, University of Cagliari, Via Marengo 2, 09123 Cagliari, Italy
{mconi,sportas,maltinti}@unica.it, james.14@tiscali.it

Abstract. The paper reports the finite element analysis of the effect of subgrade cavities on urban pavements. The study starts after a critical collapse event in 2008 in Cagliari (Italy), where a 110 m^3 sinkhole suddenly opened up, swallowing one car on an urban street. The cavity, originated by water network failure, occurred in the urban area built in a zone of abandoned limestone quarries. Pressured water erodes the subsurface and effortlessly flows through rock debris voids. The cavity grows until the weight of the above materials and traffic load trigger a collapse of the pavement. In order to evaluate the effect on the dimensions' stress field and the cavity's location below the pavement, a parametric study of the finite elements was carried out with ANSYS® software. In a section of 25 x 10 m, which comprises the road pavement and the adjacent buildings, the FEM mesh includes not linear materials and the presence in the subgrade of a circular cavity with a variable radius (0.30 ÷ 1.80 m), depth (0.50 ÷ 3.00 m) and loads (0 t, 4 t, and 8 t). The F.E. simulations' results define the pavement's bearing capacity and the developed plastic yielding of the subgrade for each condition analyzed. No trivial cavity collapse conditions and mechanisms have been discussed in detail. The results show how the effects of the dimension and position of the cavity are not linear. Small and deep cavities collapse immediately with depth increases but with progressively smaller effects on the surface. Larger and superficial cavities are critical, and the vehicular load significantly affects the superficial cavities. Future research may address how these events may affect the road network.

Keywords: Asphalt pavement · Sinkhole · FEM simulation · Stress-strain effects · Underground · Bearing capacity

1 Introduction

A rising number of failures have been reported in the last decade on the urban streets in Italy related to underground cavities and sinkholes. To ensure safety conditions and avoid pavement collapses, the evaluation of the underground cavities became a priority [1–4].

Tomita et al. (1995) developed a detection method and surveyed Japan to identify and understand the nature of subsurface voids. The Authors report more than 2.000 pavement failures per year caused by voids in Tokyo. About 200 detected voids (through GPR and

© The Author(s), under exclusive license to Springer Nature Switzerland AG 2023
O. Gervasi et al. (Eds.): ICCSA 2023 Workshops, LNCS 14111, pp. 244–259, 2023.
https://doi.org/10.1007/978-3-031-37126-4_17

borehole camera) were classified based on the volume (1.0 ÷ 4.0 m^3) and thickness (0.2 ÷ 1.0 m) under the pavement.

The underground cavities may be natural or artificial and generated from different phenomena such as water-soluble materials, mining activity, digging of the subsurface utility networks, and related actions of soil excavation [5–8]. Moreover, the urban development concern mainly regions of previous excavation human activities [9].

The potential presence of cavities must be considered in the pavement to design safe roads [10].

Several studies [5–9], and many others have been carried out on the identification and characterization of cavities, but few studies are available in the literature regarding design and evaluation criteria in pavement design. In recent years, Lee (2018) [10] has reported a 3D finite element parametric study varying cavity dimension, deep pavement thickness, and HMA stiffness, assuming the critical conditions regarding surface deflections and tensile strains.

Choi et. Al (2018) [11] extends the research developing procedures on the risk assessment in Japan for asphalt pavements due to the subsurface cavity. This relevant study considers a rectangular cavity and materials characterized by the modulus of the asphalt, subbase, and subgrade subject on a 40 kN load applied on one circular loading plate. The research pointed out how tensile strain depends primarily on the cavity depth and A.C. modulus. However, different cavity shapes, cohesive elastic-plastic subgrade, or visco-elastic A.C. proprieties can be significant in different situations. The superimposed effect of the two wheels of the axle load and the location concerning cavity position can affect the critical pavement response. Moreover, failure can also occur when the pavements have no load or with only cars loaded [12].

An important aspect concerns the evolution of the process before they evolve into dangerous pavement failures. The migration of loose material begins with an air pocket that moves upwards, increasing dimension due to the additional material being washed away. The air void moves upwards because the ceiling of the cavity falls on the floor, leaving the new ceiling uncovered. The process continues until the resisting layers of the pavement are encountered. In cold climatic conditions, the asphalt pavement could maintain enough bearing capacity to support the vehicles, while during hot weather, the stiffness of HMA drops drastically, and the pavement capability is significantly lowered [4]. The collapses remain latent in winter and reach a critical state during the summer, as Tomita et al. survey [6] pointed out.

Some relevant studies concern the cavity effect on the bearing capacity of footing [13–17].

Wang and Badie (1985) [18, 19] investigated the bearing capacity of shallow foundations on the underground cavity by 3D finite element model (FEM). The simulations point out a critical condition only for the void above the critical depth, which is not a constant. It depends on the shapes of the cavity, orientation and size, soil type, and footing dimensions. In this condition, the bearing capacity of the footing decreases the closer the cavity becomes.

Azam et al. (1997) [20] studied the bearing capacity of strip footing in two-layer soils by elastoplastic 2D FEM. The analysis provides the progress of plastic yielding

and the ultimate bearing capacity for a wide range of cavity conditions and soil layers type,

Some theoretical and experimental studies investigated the mitigation methods to improve spread footing capacity above the voids. Das and Khing (1994) [21] built and tested a two layers laboratory model with a rectangular void below the foundation. The bearing capacity is reduced and can significantly increase with a geogrid layer.

In 2009 analogous study in the laboratory, developed by Sireesh et al. [22], investigated a circular footing over a circular void. They report considerable bearing enhancements providing a geo-cells reinforcement between the footing and the void.

Fang and Li (2011) [23] use elastic-plastic dynamic FEM to evaluate the differential settlement of the half-filled and half-dug embankment under the traffic load. The deformations of the asphalt layers under different conditions have been considered to identify the critical condition and settlement of the pavement.

Several Authors pointed out how nonlinear FEM analysis affects asphalt pavement stress-strain response.

Deng et al. (2004) developed an elastic-plastic dynamic F.E. model to evaluate the differential settlement of the half-filled and half-dug embankment under automobile load and subsoil consolidation.

Al-Qadi, Wang, and Coni (2010, 2013) [25, 26] studied the response of an instrumented runway asphalt pavement and developed 3D finite element simulations considering A.C. layers with viscoelastic proprieties and introducing elastoplastic characteristics in the subgrade and subbase materials. The pavement layers were equipped with 149 instruments (LVDT for displacement, pressure cells, TDR for moisture content, T-thermocouples, and strain gauges), monitoring in real-time the effects of landing and take-off in the pavement. The data collected from over 48000 movements during 2009–2011 have been used to validate the advanced pavement model. Good agreements were achieved at various locations, comparing measured responses from field instrumentation and calculated pavement responses.

Based on the results and remarks of these researchers, the papers summarize the case of the study and describe the FEM modeling and results.

Future research may investigate how these events may affect the road network. Some Authors pointed out how developing the model architecture of traffic control and microsimulation modeling is a valuable tool to analyze the road urban transport network and its capacity through a dynamic assignment model [32–35]. In addition, early simulation can address and minimize road network vulnerability in areas with sinkhole risk.

2 Case Study

The research started when a critical collapse occurred in August 2008 in Cagliari (Italy), where a 110 m^3 sinkhole suddenly opened up, swallowing one car on an urban street (Fig. 1). The cavity, originated by water network failure, occurred in the urban area built in a zone of abandoned limestone quarries. Pressured water erodes the subsurface and effortlessly flows through rock debris's voids. The cavity grows until the weight of the above materials and traffic load trigger a collapse of the pavement.

Similar events in the area have occurred in the last decades, involving buildings and urban streets (Fig. 2). The presence of cavities below the road level in the area is well known, and their evolution caused detachments and collapses.

In 2007, a large mass of about 8 tons detached from the roof of a cavity determining the permanent limitation to road traffic. In 1993, a large cavity ($4.0 \times 13.0 \times 3.0$) suddenly opened on the roadside, causing building flood, structural failures and traffic restrictions. A critical collapse occurred on May 12, 1987.



Fig. 1. The collapse occurred on August 11, 2008

A chasm of similar size dragged the facade of a building and part of the roadway. In August 1961, a cavity collapse caused severe structural failure, an entire building was demolished, and a large roadside was closed to traffic. A more significant number of events caused minor damage but manifested a widespread and high-risk problem.

The geology of the area presents several outcrops of Cenozoic and Neozoic formations. It consists mainly of well-cemented arenaceous benches, alternating with incoherent sand and layers of conglomerates with Paleozoic rock clusters and limestone and marly sandstones that emerge in the urban landscape.

Marly - yellowish arenaceous limestone, badly stratified with thicknesses up to 50 m, is also present, sometimes overlaid by biocalcarenites. The basal part is characterized by slumping, faults, erosion surfaces, and different intrusions with variable thicknesses of 0 and 40 m.

The geotechnics problems of the area affect the building's stability and road regularity, often resulting from inadequate foundations and construction methods, considering the substrate's heterogeneous and poor geotechnical characteristics.



Fig. 2. The area affected by the landslide hazard and the event location.

During the post-war reconstruction and urban expansion, the area was affected by widespread construction without considering the plane-altimetric remodeling that occurred to fill and regularize the artificial morphological irregularities.

In the first half of the 20th century, the area underwent intense activity to extract rocks destined for the cement industry. The closure of the mining activity was gradual until the complete disposal in 1977 (Fig. 3).

In the last 20 years, the surveys highlighted a high geomechanical anisotropy, manifested by several subsidence and settlements of buildings foundations and investigated by an extensive survey campaign conducted between 2008 and 2011.

These included gravimetric geophysical tests, seismic tomographies, deep prospecting and superficial trenches surveys, penetrometer tests, exploration wells, and building inspections, laboratory tests (humidity, monoaxial compression, limits, Atterberg, particle sizes, classifications, cutting tests, etc.), carried out first on a large scale and then concentrated in the areas identified at greater risk.

The surveys, carried out at depths between 10 and 45 m, show the quarry debris overlay with thicknesses ranging between 1.80 to 25.0 m. These materials represent the greatest geostatic criticality of the area, with non-stabilized, non-densified soils predisposed to further settling, locally soft and porous, with primary voids generated by the laying technique.

These materials are susceptible to the action of groundwater, especially those under pressure resulting from water losses.

The traces and slopes of the quarry processing planes, built to facilitate the transport of the extracted material, are essential for understanding the underground water flow of the infiltration waters.

The geotechnical plane-altimetry variability makes complex the modeling of the subsoil. Therefore, it is fundamental to know the thicknesses of the debris and their

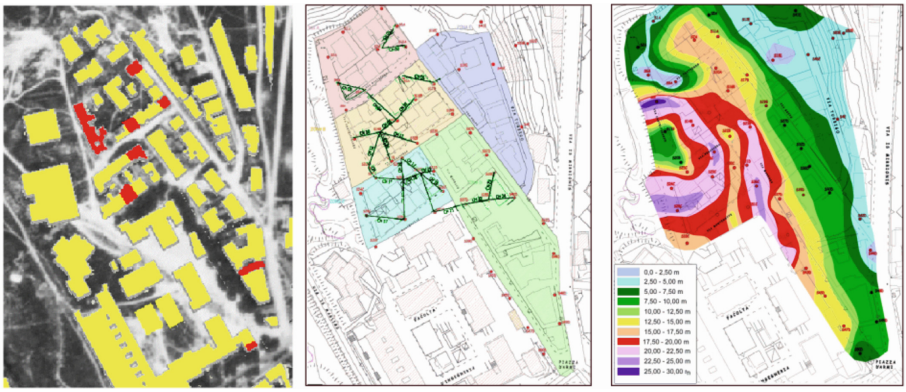

Fig. 3. On the left: aerial photo in 1946 shows the sign of quarry activity and the later building's construction (yellow). In red are the damaged buildings. In the middle: the survey and seismic topographies locations. On the right: the reconstructed thickness of the quarry debris. (Color figure online)

syngeneic porosity, which is often crossed by underground water flows due to percolation or to the losses water network.

The solution identified in order to mitigate the risk involved the construction of a technological tunnel below the roads, waterproof and easy inspection, within which to house all the utilities (white water, sewage, telecommunications, electricity, gas, public lighting, rainwater network, etc.) equipped with sensors to immediately detect leaks and activate specific maintenance. Moreover, the realization of rigid road pavement maintains the integrity of the road pavement even in case of sinking. At the same time, the Cagliari Municipality, up to the implementation of the technological tunnel, has ordered building and urban transformation restrictions (Fig. 4).

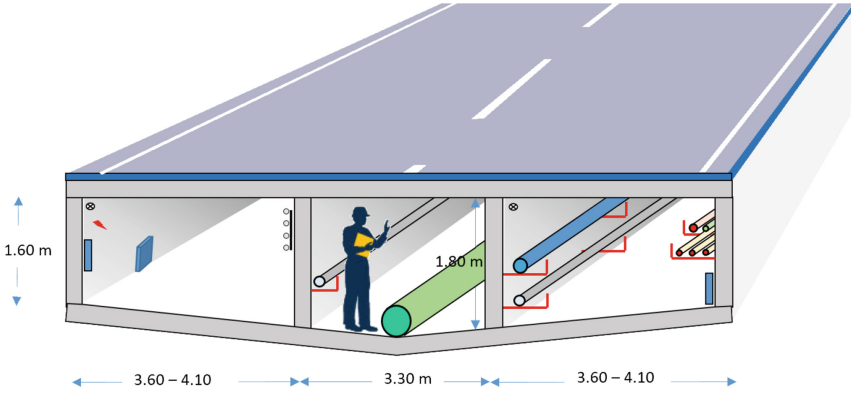

Fig. 4. The cross-section of the sub-services tunnel

Between 2013 and 2014, Cagliari Municipality planned, designed, and financed four sub-service tunnels under the roads. The construction of the first tunnel, concerned with securing the road affected by the collapse of 2008, started in 2015. After excavating the whole road section up to a depth of 2.50 m, the bottom and sides of the dugout have been consolidated with injections of cement grouting. The reinforced concrete foundations, walls, and roof define three compartments that house all the underground services and safely manage any water leaks. The tunnel was completed in 2017, as shown in Fig. 5. The second tunnel work began in 2018, and it is under construction.



Fig. 5. The construction site and works for the first subservice tunnel.

3 Research Methodology

During the study for a proper consolidation method, an important aspect has been to evaluate the level of risk connected to the presence of a cavity. In order to calculate the effect on the stress and strain of the dimensions, the shape, and the location of the cavity below the pavement, a parametric study of the finite elements was carried out with ANSYS® software, considering the influence of asphalt and granular materials nonlinearity [24].

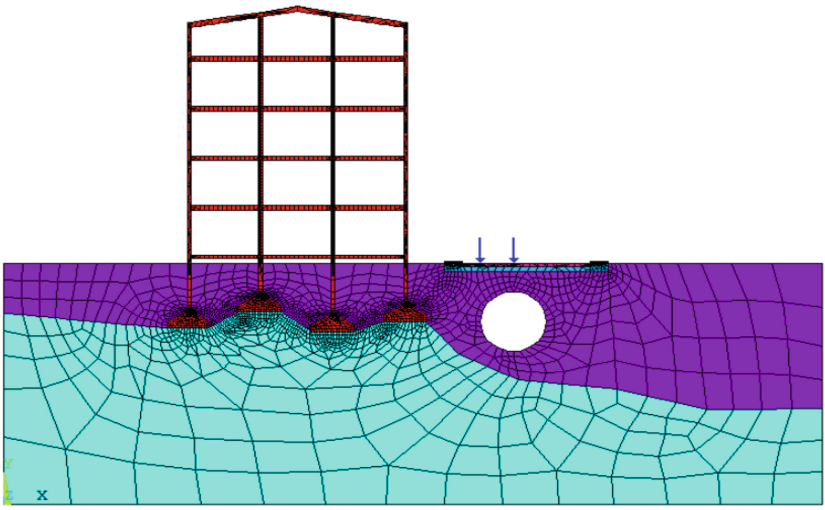

Fig. 6. 2D FEM section

Several Authors investigate the sinkhole phenomena with the finite element method [28–30].

In a section of 25 × 10 m, which comprises the road pavement and the adjacent buildings, the 2D FEM mesh (Fig. 6) includes not-linear materials and the presence in the subgrade of different shapes of a cavity (triangular, square, rectangular, and circular) with variable dimension (0.10 ÷ 1.80 m), depth (0.40 ÷ 4.00 m) and loads (0 t, 4 t, and 8 t).

Each combination generates different conditions in the subgrade and the pavement layers in terms of a) superficial deflections, b) stresses, and c) strains.

a) The cumulated plastic deformation determines a superficial permanent deflection as a function of traffic load spectra. In the study, the total permanent deflection δ_p of 10 mm, under wheel axis and standard traffic, was assumed as the limit to define a critical condition for superficial planarity. The value of 10 mm is the same limit assumed for rutting in road management.
b) The magnitude of shear stress compared to shear strength has been adopted to estimate if the soil can sustain the stress. The shear resistance of soil is a result of friction (ϕ) and cohesion (c), according to Navier–Coulomb criterion:

$$\tau_{cr} = c + \sigma \tan \phi \tag{1}$$

The normal stress has a stabilizing consequence, increasing the shear stress strength. Mohr theory defines, in the shear surface, the relationship between shear and normal stresses. The following equations can express them:

$$\sigma = \frac{\sigma_1 + \sigma_3}{2} + \frac{\sigma_1 - \sigma_3}{2} \cos 2\theta \tag{2}$$

$$\tau = \frac{\sigma_1 - \sigma_3}{2} \sin 2\theta \tag{3}$$

where σ_1 and σ_3 are the major and minor principal stress and θ the angle between major principal stress and shear plane direction. Applying trigonometric functions, they can be expressed by:

$$\left(\sigma - \frac{\sigma_1 + \sigma_3}{2}\right)^2 + \tau^2 = \left(\frac{\sigma_1 - \sigma_3}{2}\right)^2 \tag{4}$$

It is possible to define the state of limit failure, combining Mohr theory and Navier–Coulomb criterion (Figure 7), when the strength line is tangent to the Mohr circle. Solving the system of equations (1) and (4) allow us to determine $\tau_{cr.}$

Many factors affect the value of c and ϕ, such as the kind of material, the morphology of the grains, and water [27]. In particular, moisture content decreases cohesion, increasing weight and pore water pressure in granular media.

Among the geotechnical data, dozens of friction and cohesion value are available in different locations and depths of the area, ranging from 23° to 29° and 4 kPa and 11 KPa for the fill materials. Also, a mean value of density (18.2 kN/m^3) and stiffness modulus (31 MPa) are available to perform F.E. simulation.

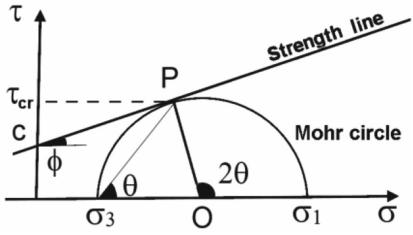

Fig. 7. Strength line and Mohr circle in σ-τ plane.

A mean value of 26° and 7.5 KPa have been introduced in Navier–Coulomb equation as well σ_1 and σ_3 values derived from F.E. simulation to estimate the shear strength. Finally, for each condition considered in a parametric analysis and for each position, τ_{cr} was compared with τ evaluated from the F.E. model at the same point.

c) The tensile strain at failure depends on the moisture content and the level of compaction. In undrained tests, well-compacted soils (100% γ_s, the maximum density of AASHTO T180 at w_{opt}, the optimum moisture content) have a typical maximum tensile strain ε_{tmax} around $0.2 \div 0.3\%$. Increasing moisture content, the ε_{tmax} grows until the maximum value of $0.7 \div 0.8\%$ for $w = w_{opt} + 6\%$ [31]. The values of the ε_{tmax} are in the range of 0.2–0.6 % and growth with the plasticity index value. The drained triaxial test exhibit very different behavior, and the ε_{tmax} is about 10 times higher. The landfill soils in the area have been mainly classified as A2-4 HRB classification, with plasticity index $Ip = 4$ and liquid limit $L.L. = 38$. According to the mean value of the soils tested in the area, it has been assumed $\varepsilon_{tmax} = 0.6\%$.

4 F.E. Results

Equivalent strains ε_t vary considerably with load, cavity depth, and size and range from 2136 to 8287 μstrain (Fig. 8).

It is relevant to note that critical conditions of εt also occur in the absence of vehicular load for small cavities and at depths of 4.0 m. However, this condition does not create

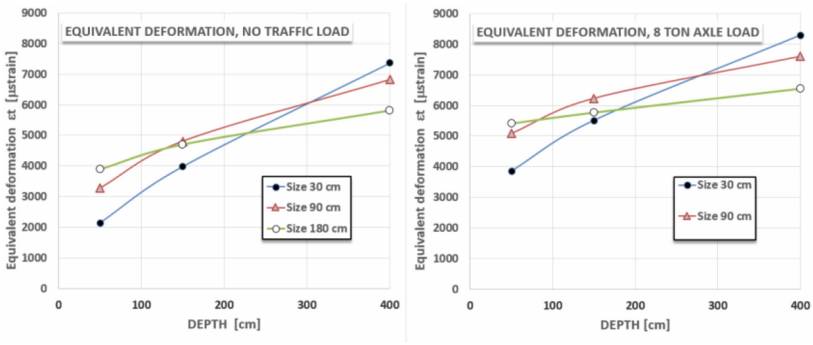

Fig. 8. Equivalent deformation with and without traffic load

critical conditions at the pavement surface because the material plastically collapsing fills the small cavity with negligible effects at the surface.

In the 30 cm cavities, as depth increases, the ε_t grows from 2150 μstrain to over 7400 μstrain, while for sizes between 90 ÷ 150 cm, the deformations are smaller, between 3200 ÷ 6990 μstrain. The following graph shows a nontrivial trend. Larger cavities are more critical but still within tolerable values of $\varepsilon t < 4000$ μstrain, compared to cavities of smaller size but placed at greater depths. With no load, ε_t is greater for cavities of large diameters near the surface and grows less rapidly than for smaller cavity sizes. Similar behavior is observed when a vehicular load is present but with ε_t values 32% greater for 4 t axles and 25% greater for 8 t axles.

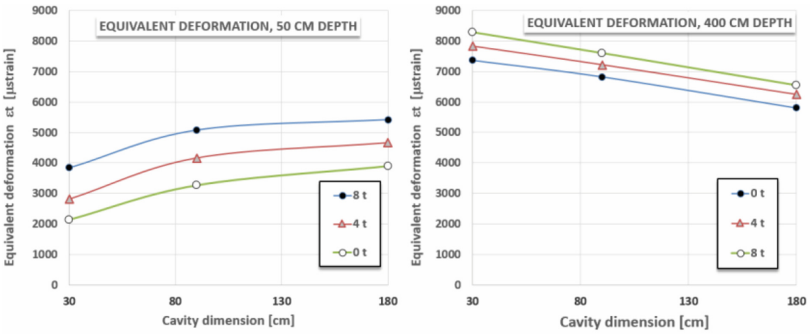

Fig. 9. Equivalent deformation for different depth cavity

The ε_t shows a monotonic decreasing behavior for surface cavities (−50 cm) and increasing diameters, while the trend is decreasing for deep cavities (400 cm) (Fig. 9). In the first case, the values are, under all conditions considered, less than 5500 μstrain. In the absence of vehicular load and only self-weight, they assume a fly of 3900 μstrain and increase by about 760 μstrain with a 4 t axle and 1520 μstrain with an 8 t axle.

The stresses also show a nontrivial trend. Without traffic loads, the maximum τ occurs with large-diameter cavities (180 cm) at small depths with 10.3 kPa values above τ_{cr}. As depth increases, the values decrease rapidly (2.3 kPa). Smaller cavities have the opposite behavior. For cavities of 90 cm, the τ grow as depth increases linearly, while small cavities of 30 cm are progressively less significant. For small depths, as load increases, the curves translate toward values of τ greater than 7.0 kPa for each 4 t increase in vehicular load. At depths greater than 150 cm, the curves tend to overlap, remaining less than τ_{cr} in each case (Fig. 10.)

For small diameters (30 cm), a critical depth of around 150 cm is highlighted by the bell curves in Fig. 11. It is observed that the maximum τ peaks at 12.0 kPa for loads of 8 t. Lower loads result in reduced peaks that are absent when only the fill's weight acts on the cavity. This particular behavior is not found in larger cavities. Whereas depth increases, the curves progressively decrease (Fig. 12).

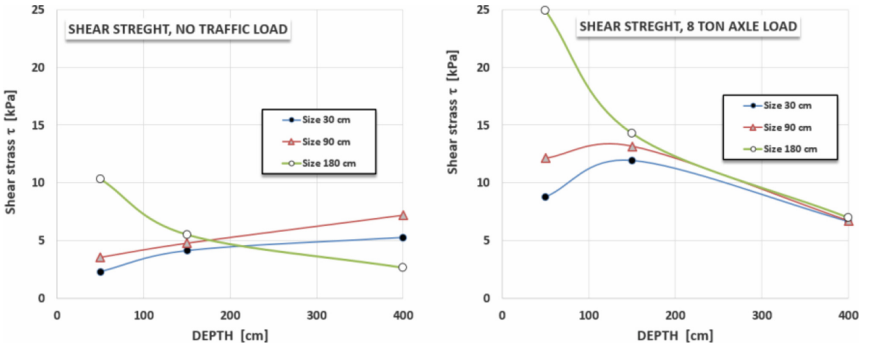

Fig. 10. Shear stress with and without traffic load

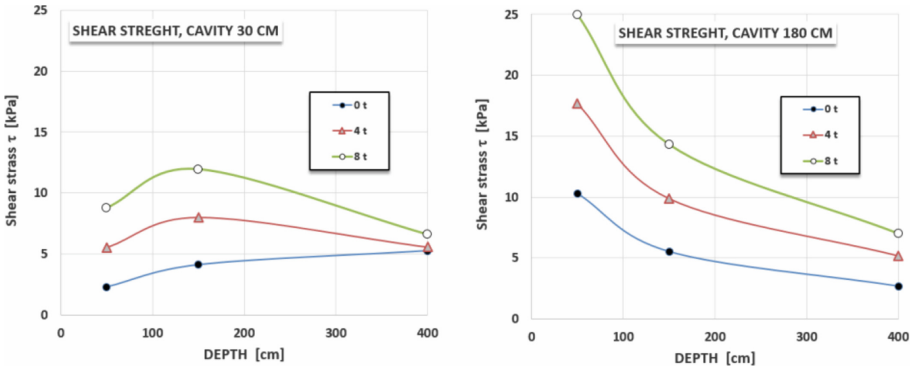

Fig. 11. Shear stress for small and large cavities

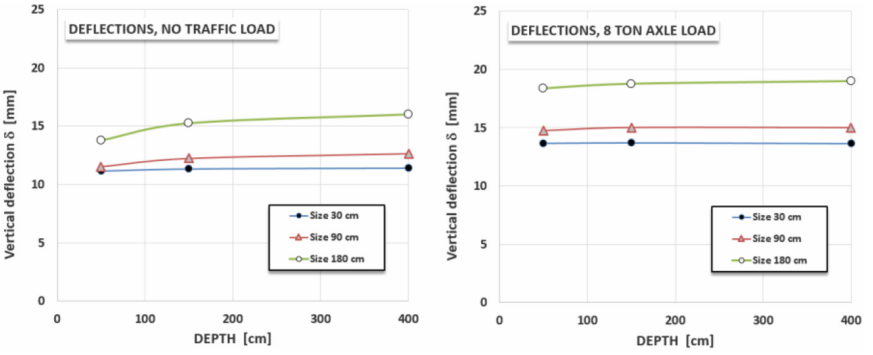

Fig. 12. Deflection with and without traffic load

In the following graphs (Figs. 13, 14, and 15), the complexity can be better represented in 3D by setting for the 3 axes the values of load, depth, and cavity size.

The vertical deflections δv have more local minimum conditions for both small and large depths. For a depth of about 150 cm, the deflections are almost indifferent to load and depth, presenting very similar values between 1.30 and 1.40 cm. The minimum values occur for depths of 150 cm, dimensions of 70 cm, and the load of 4 t.

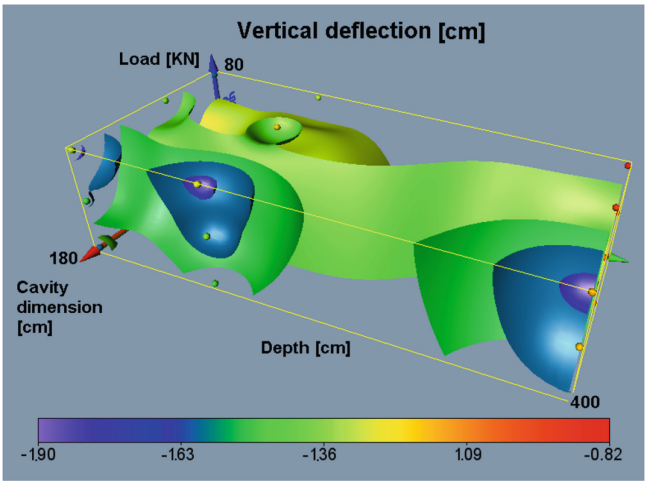

Fig. 13. Vertical deflection in 3D vs. loads, cavity dimension, and depth

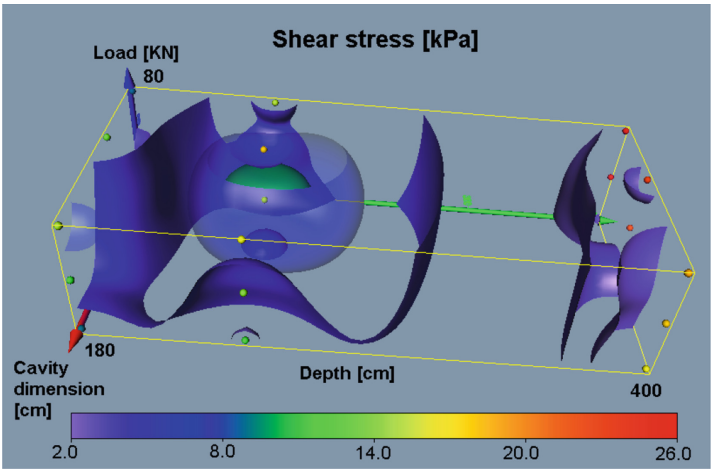

Fig. 14. Shear stress in 3D vs. loads, cavity dimension, and depth

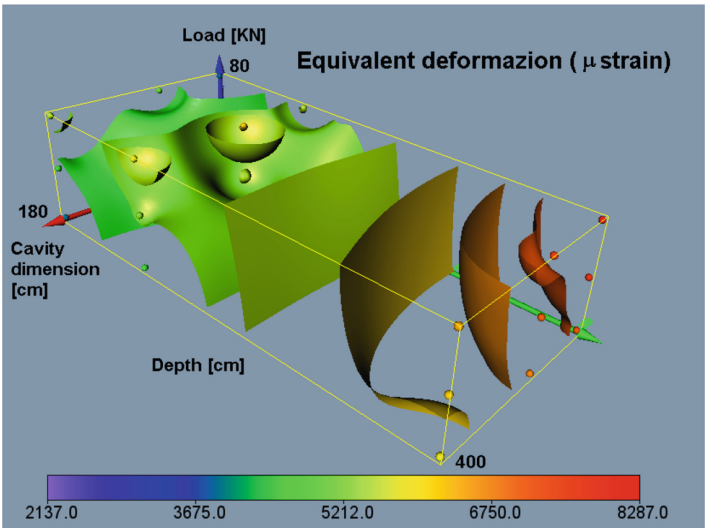

Fig. 15. Equivalent deformations in 3D vs. loads, cavity dimension, and depth

5 Conclusion

The paper reports the finite element analysis of the effect of subgrade cavities on urban pavements.

The detailed numerical investigation showed how an underground cavity under the road pavements could induce the failure event in no trivial. A numerical model based on finite element analysis and elastoplastic materials was implemented to determine the failure mechanism and the critical cavity characteristics.

The results show that underground cavities under urban roads play an essential role in the collapse and deformation phenomena of the road surface. It is predicted that gravity may damage lead to crises for cavities greater than 1.50 m, thus destabilizing the roadway's surface and, in extreme cases leading to its collapse.

This study can provide predictive analysis methods for hidden cavities and as a case study to prevent similar geological hazards in the study area.

The study starts after a critical collapse event in 2008 in Cagliari (Italy), where a 110 m^3 sinkhole suddenly opened up, swallowing one car on an urban street. The cavity, originated by water network failure, occurred in the urban area built in a zone of abandoned limestone quarries. Pressured water erodes the subsurface and effortlessly flows through rock debris's voids. The cavity grows until the weight of the above materials and traffic load trigger a collapse of the pavement.

In order to evaluate the effect on the stress and strain field of the dimensions and the location of the cavity below the pavement, a parametric study of the finite elements was carried out with ANSYS® software. In a section of 25 × 10 m, which comprises the road pavement and the adjacent buildings, the FEM mesh includes not linear materials and the presence in the subgrade of a circular cavity with a variable radius (0.30 ÷ 1.80 m), depth (0.50 ÷ 4.00 m) and loads (0 t, 4 t, and 8t).

No trivial cavity collapse conditions and mechanism have been discussed in detail. The results show how the effects of the dimension and position of the cavity are not linear. Small and deep cavities collapse immediately with depth increases but with progressively smaller effects on the surface. Larger and superficial cavities are more critical, and the vehicular load has more significant effects on the superficial cavities.

Equivalent deformation ε_t varies with load, cavity depth, and size and ranges from 2136 to 8287 μstrain. Critical values of ε_t also occur in the absence of vehicular load for small cavities and at depths of 4.0 m. However, this condition does not create critical conditions at the pavement surface because the material plastically collapsing fills the small cavity with negligible effects at the surface.

In the 30 cm cavities, as depth increases, the ε_t grows from 2150 μstrain to over 7400 μstrain, while for sizes between $90 \div 150$ cm, the deformations are smaller, between $3200 \div 6990$ μstrain. With no load, ε_t is greater for cavities of large diameters near the surface and grows less rapidly than for smaller cavity sizes. Similar behavior is observed when a vehicular load is present but with ε_t values about 30% greater.

The ε_t shows a monotonic decreasing behavior for surface cavities (-50 cm) and increasing diameters, while the trend is decreasing for deep cavities. The stresses also show a nontrivial trend. Without traffic loads, the maximum τ occurs with large-diameter cavities at small depths. As depth increases, the values decrease rapidly. Smaller cavities have the opposite behavior. For average cavities the τ grow as depth increases linearly, while small cavities are progressively less significant.

For small diameters, a critical depth of around 150 cm is highlighted by Fem simulation. This particular behavior is not found in larger cavities. Whereas depth increases, the curves progressively decrease. The 3D maps δ_v, τ and ε_v versus depth and size of cavity and load can better represent the behavior complexity.

Acknowledgments. The Road Department of the Cagliari Municipality in Italy supports the research. The authors want to acknowledge Dr. D. Olla and Dr. A. Masala for their technical support during the in situ investigations.

References

1. Zhao, Y., Shi, Y., Wua, F., Sun, R., Feng, H.: Characterization of the sinkhole failure mechanism induced by concealed cave: a case study. Eng. Fail. Anal. **119**, 105017 (2021)
2. Debasis, D., Choi, S.O., Shin, H.S.: Analysis of sinkhole formation over abandoned mine using active-passive finite elements. Tunnel Undergr. Space 14(6), 441–422 (2004). Journal of Korean Society for Rock Mechanics
3. Tao, X., Ye, M., Wang, X., Wang, D., Castro, R.P., Zhao, J.: Experimental and numerical investigation of sinkhole development and collapse in Central Florida (2015).
4. Shalev, E., Lyakhovsky, V., Yechieli, Y.: Salt dissolution and sinkhole formation along the Dead Sea shore. J. Geophys. Res. Solid Earth **111**(B3), B03102 (2006)
5. Zam, G., Jao, M., Wang, M.C.: Cavity effect on the stability of strip footing in two-layer soils. Geotech. Eng. **28**(2), Southeast Asian Geotechnical Society, ISSN: 0046-5828 (1997)
6. Al-Jazaairry, A.A., Sabbagh, T.T.: Effect of cavities on the behaviour of strip footing subjected to inclined load. Int. J. Civ. Environ. Struct. Constr. Archit. Eng. **11**(3), 292–298 (2017)

7. Baryakh, A.A., Fedoseev, A.K.: Sinkhole formation mechanism. J. Min. Sci. **47**(4), 404–412 (2011)
8. Tharp, T.: Cover-collapse sinkhole formation and soil plasticity. In: Beck, B.F. (ed.) Sinkholes and The Engineering and Environmental Impacts of Karst; 6–10 Sept. 2003; Huntsville, Alabama, pp. 110–123 . ASCE Publishing (2003)
9. Badie, M.C., Wang: Stability of spread footing above void in clay. J. Geotech. Eng.-ASCE **110**(11), 1591–1605 (1984)
10. Crapps, D.K.: The effects of cavities upon foundation design & construction. In: Art of Foundation Engineering Practice. ASCE (2010)
11. Kawana, F., Kubo, K., Ueda, N., Takeuchi, Y., Matsui, K.: Study of the cavity problem under the pavement caused by the earthquake. In: Richard Kim, Y. (ed.) Asphalt Pavements, 1st edn. (2014)
12. Tomita, H., Tada, H., Nanbu, T., Chou, K., Nakamura, T., McGregor, T.: Nature and Detection of Void-Induced Pavement Failures, Transportation Research Record 1505, Pavement Design, Management, and Performance. National Academy Press, Washington D.C. (1995)
13. Kovacs, A., Morey, R.M.: Detection of cavities under concrete pavement, U.S. Army Corps of Engineers CRREL, Cold Regions Research Engineering Laboratory, REPORT 8/18 (1983). https://apps.dtic.mil/dtic/tr/fulltext/u2/a131851.pdf
14. Gucunski, N., Shokouhi, P.: Detection and characterization of cavities under the airfield pavements by wavelet analysis of surface wave. In: 2004 FAA Worldwide Airport Technology Transfer Conference, Atlantic City, USA (2004). https://www.researchgate.net/publication/228563347_Detection_and_characterization_of_cavities_under_the_airfield_pavements_by_wavelet_analysis_of_surface_waves
15. Abbasghorbani, M., Bamdad, A.: Nondestructive detection of voids under airfield pavement. In: Proceedings of the 10th International Conference on the Bearing Capacity of Roads, Railways and Airfields (BCRRA 2017), 28–30 June 2017, Athens, Greece (2017)
16. Lee, W.S., Woo Choi, Y., Jong Lee, H., Mun Park, H.: Sensitivity analysis on the effect of cavity in structural capacity of asphalt pavement using finite element analysis. In: Proceedings of the Korean Society of Road Engineers Conference, Spring Conference (2018). http://db.koreascholar.com/article?code=348335
17. Choi, Y.W., Park, H.M., Kim, Y.T., Lee, W.S., Lee, H.J.: A risk assessment of asphalt pavement for depression and cave-in caused by a subsurface cavity. Int. J. Pavement Eng. **21**, 1092–1102 (2018). https://doi.org/10.1080/10298436.2018.1520231
18. Wang, M.C., Badie, A.: Effect of underground void on foundation stability. J. Geotech. Eng. **111**(8), 1008–1019 (1985)
19. Badie, A., Wang, M.C.: Stability of spread footings above void in clay. J. Geotech. Eng. ASCE **110**(11), 1591–1605 (1984)
20. Azam, G., Jao, M., Wang, M.C.: Cavity effect on stability of strip footing in two-layer soils. Geotech. Eng. J. SEAGS **28**(2) (1997). Ed. Southeast Asian Geotechnical Society, ISSN 0046–5828 (1997)
21. Das, B.M., Khing, K.H.: Foundation on layered soil with geogrid reinforcement effect of a void. Geotext. Geomembr. **13**(8), 545–553 (1994)
22. Sireesh, S., Sitharam, T.G., Dash, S.K.: Bearing capacity of circular footing on geocell-sand mattress overlying clay bed with void. Geotext. Geomembr. **27**(2), 89–98 (2009)
23. Fang, S., Li, H.: Mechanical analysis of asphalt pavement structure affected by underground pipeline of urban road. J. Hefei Univ. Technol. 2011-04 (2011)
24. Deng, W., Zhang, X., Chen, B., Yan, S.: Nonlinear FEM analysis of influence of asphalt pavement under non-homogenous settlement of roadbed. China J. Highw. Transp. 2004-01 (2004)

25. Wang, H., Al-Qadi, I.L., Portas, S., Coni, M.: Three-dimensional finite element modeling of instrumented airport runway pavement responses. In: TRB Transportation Research Board, 92th Annual Meeting, Washington, 12–17 January 2013
26. Al-Qadi, I.L., Portas, S., Coni, M., Lahouar, S.: Runway pavement stress and strain experimental measurements, Transportation Research Record, No. 2153 (2010)
27. Vanicek, I.: The importance of tensile strength in geotechnical engineering. ACTA Geotechnica Slovenica (2013). http://www.fg.uni-mb.si/journal-ags/pdfs/AGS_2013-1_article_1.pdf
28. Ahmed, M.: Experimental and numerical modeling of sinkhole collapse. In: Proceedings of the Transportation Research Board 92nd Annual Meeting, 13–17 Jan 2013, Washington, D.C (2013)
29. Shalev, E., Lyakhovsky, V.: Viscoelastic damage modeling of sinkhole formation. J. Struct. Geol. **42**, 163–170 (2012)
30. Caudron, M., Emeriault, F., Kastner, R.: Collapses of underground cavities and soil-structure interactions: experimental and numerical models. In: Proceedings of the 1st Euro Mediterranean Symposium on Advances on Geomaterials and Structures, 3–5 May 2006, Hammamet, Tunisia (2006)
31. Jin, W., Wang, W., Wang, B., Pan, Z.: Shear failure criteria of soft soil under complex stress condition. In: Qi, L. (ed.) ISIA 2010. CCIS, vol. 86, pp. 17–23. Springer, Heidelberg (2011). https://doi.org/10.1007/978-3-642-19853-3_3
32. Torrisi, V., Ignaccolo, M., Inturri, G.: The microsimulation modeling as a tool for transport policies assessment: an application to a real case study. In: AIP Conference Proceedings, vol. 2611, no. 1, p. 060006. AIP Publishing LLC (2022)
33. Bourguignon, F., Spadaro, A.: Microsimulation as a tool for evaluating redistribution policies. J. Econ. Inequality **4**, 77–106 (2006). https://doi.org/10.1007/s10888-005-9012-6
34. Torrisi, V., Ignaccolo, M., Inturri, G.: Innovative transport systems to promote sustainable mobility: developing the model architecture of a traffic control and supervisor system. In: Gervasi, O., et al. (eds.) ICCSA 2018. LNCS, vol. 10962, pp. 622–638. Springer, Cham (2018). https://doi.org/10.1007/978-3-319-95168-3_42
35. Torrisi, V., Ignaccolo, M., Inturri, G.: Analysis of road urban transport network capacity through a dynamic assignment model: validation of different measurement methods. Transp. Res. Procedia **27**, 1026–1033, ISSN: 2352-1465 (2017). https://doi.org/10.1016/j.trpro.2017.12.135